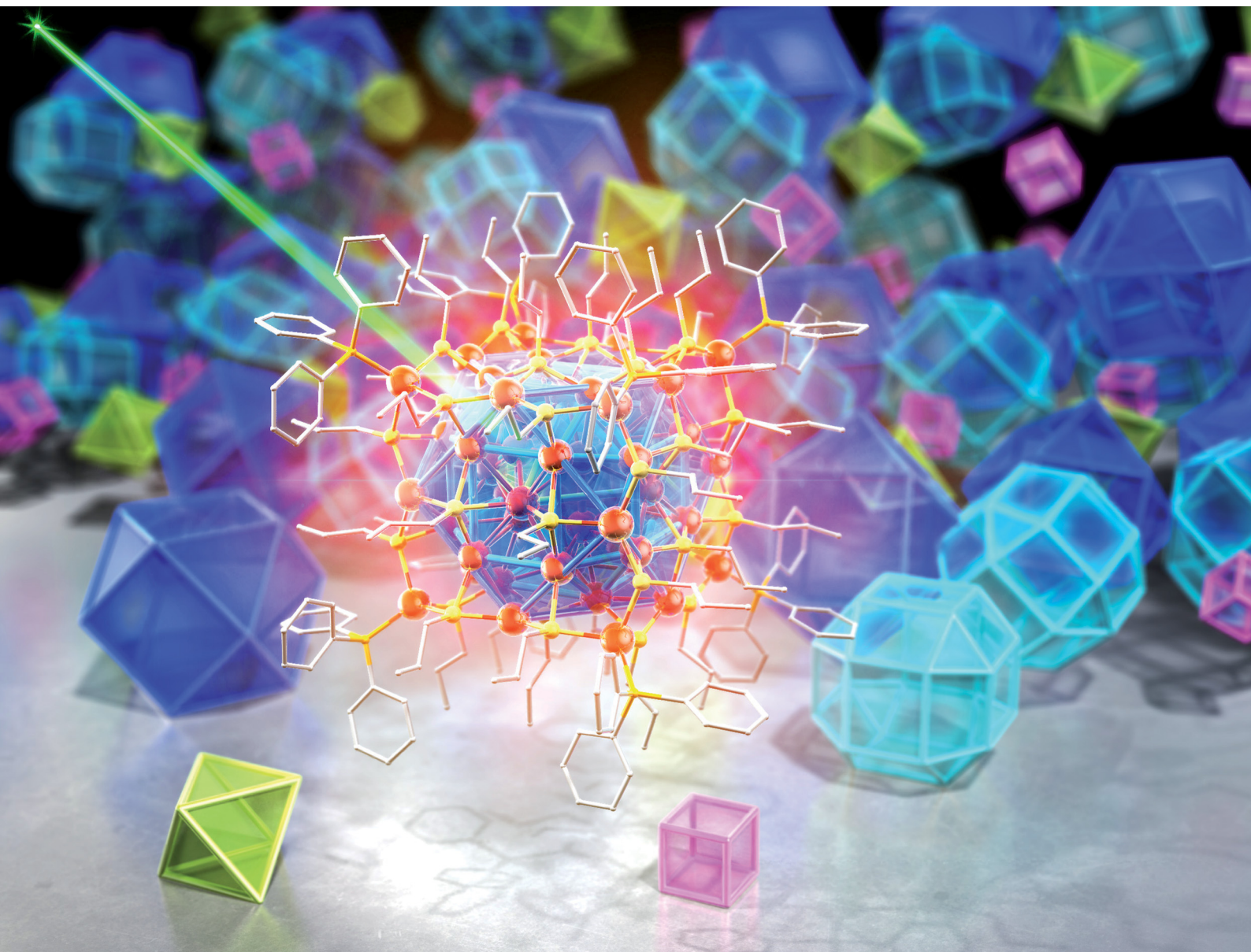


ChemComm

Chemical Communications

rsc.li/chemcomm



ISSN 1359-7345

COMMUNICATION

Saikat Das, Song Wang, Yuichi Negishi *et al.*
Nested Keplerian architecture of $[\text{Cu}_{58}\text{H}_{20}(\text{SPR})_{36}(\text{PPh}_3)_8]^{2+}$
nanoclusters



Cite this: *Chem. Commun.*, 2023, 59, 9336

Received 13th April 2023,
Accepted 23rd June 2023

DOI: 10.1039/d3cc01811c

rsc.li/chemcomm

Nested Keplerian architecture of $[\text{Cu}_{58}\text{H}_{20}(\text{SPr})_{36}(\text{PPh}_3)_8]^{2+}$ nanoclusters†

Sourav Biswas,^a Sakiat Hossian,^a Taiga Kosaka,^a Jin Sakai,^a Daichi Arima,^b Yoshiki Niihori,^a Masaaki Mitsui,^b De-en Jiang,^c Saikat Das,^a Song Wang^{*d} and Yuichi Negishi^{*,a}

This article explores the challenges in synthesizing highly symmetric Cu(I)–thiolate nanoclusters and reports a nested Keplerian architecture of $[\text{Cu}_{58}\text{H}_{20}(\text{SPr})_{36}(\text{PPh}_3)_8]^{2+}$ (Pr = $\text{CH}_2\text{CH}_2\text{CH}_3$). The structure is made up of five concentric polyhedra of Cu(I) atoms, which create enough space to accommodate five ligand shells all within a range of 2 nm. This fascinating structural architecture is also linked to the unique photoluminescence properties of the nanoclusters.

The main polyhedra, or three-dimensional shapes with flat polygonal faces, have fascinated people for centuries. The study of polyhedra dates back to ancient civilizations who discovered two classes of convex equilateral polyhedra containing 5 Platonic and 13 Archimedean solids, which intrigued them with their symmetry and mathematical properties.^{1–3} Later on, Johannes Kepler discovered a third class, the rhombic polyhedra.¹ Over time, the study of polyhedra has extended beyond mathematics and has become an essential tool in a variety of disciplines, including architecture, physics, biology, and chemistry. In chemistry, polyhedral models have been used to study the structure of molecules, a critical aspect for understanding their behavior and function, *i.e.*, correlating their structures and properties. The study of molecular geometry is essential to various branches of chemistry. Polyhedral models allow researchers to visualize and analyze the structure of

complex molecules, providing insights into their fascinating geometric properties and wide range of applications.^{4–8}

Since the discovery of buckminsterfullerene (C_{60}), researchers have been inspired to build a miniaturized form of polyhedral symmetric structures/clusters.^{9,10} Despite several attempts, the family of such clusters still remains incomplete, and synthesizing highly symmetric Cu nanoclusters (NCs) has proven to be challenging.^{11,12} Since the beginning of Cu NC research, various Cu NCs have been reported.¹¹ Attempts have been made with Cu–thiolate NCs to match the structural arrangement of Au and Ag–thiolate NCs.¹¹ However, highly-symmetric Cu–thiolate NCs remain unknown due to issues related to the variable oxidation states of Cu atoms and its lower half-cell reduction potential than both Au and Ag.^{13,14} While some reports of such clusters exist in the literature, concentrically nested architectures are still rare.^{15–22} In this study, we report a nested Keplerian architecture of $[\text{Cu}_{58}\text{H}_{20}(\text{SPr})_{36}(\text{PPh}_3)_8]^{2+}$ (Pr = $\text{CH}_2\text{CH}_2\text{CH}_3$) (Cu_{58}) NCs under these circumstances.

To synthesize Cu_{58} NCs, 0.16 mmol of $\text{Cu}(\text{CH}_3\text{CN})_4\text{BF}_4$ was first treated with 0.19 mmol of PPh_3 in an acetonitrile/chloroform (4 : 1) mixture at room-temperature. Next, HSPr was added to the mixture, and a reducing agent (NaBH_4) was dissolved in methanol and added drop-wise by maintaining the solution temperature at 5–10 °C, causing the solution to change from colorless to deep red. After the reaction was completed, the resulting dry red precipitate was dissolved in a chloroform/hexane (V : V = 1 : 1) solution and left to crystallize under ambient conditions for 10 days. Eventually, deep red-colored box-shaped crystals were obtained and the color and shape were confirmed by both optical and scanning electron microscopy images of the crystals (Fig. S1, ESI†). The presence of the ternary solvent medium during the reaction is crucial here, which controls the reduction process and growth of the crystals.²³ While adding chloroform to the reaction mixture was previously done to provide chloride ions for use as ligands, in this case, there was no such dissociation involved.²⁰ However, without chloroform, crystal isolation was not possible. Through the drop-wise addition of the reducing agent at lower

^a Department of Applied Chemistry, Faculty of Science, Tokyo University of Science, Kagurazaka, Shinjuku-ku, Tokyo 162-8601, Japan. E-mail: saikatdas@rs.tus.ac.jp, negishi@rs.tus.ac.jp

^b Department of Chemistry, College of Science, Rikkyo University, Toshima-ku, Tokyo 171-8501, Japan

^c Department of Chemical and Biomolecular Engineering and Department of Chemistry, Vanderbilt University, Nashville, TN 37235, USA

^d Hefei National Research Center for Physical Sciences at the Microscale, School of Chemistry and Materials Science, University of Science and Technology of China, Hefei, Anhui 230026, P. R. China. E-mail: wsong09@ustc.edu.cn

† Electronic supplementary information (ESI) available: For details of instrumentation, synthesis and crystallographic parameters. CCDC 2255364. For ESI and crystallographic data in CIF or other electronic format see DOI: <https://doi.org/10.1039/d3cc01811c>



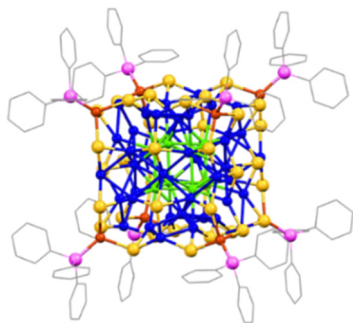


Fig. 1 Crystal structure of a $[\text{Cu}_{58}(\text{SPr})_{36}(\text{PPh}_3)_8]^{2+}$ NC. Color legend: Cu, light green, blue and brown; S, yellow; P, violet; and C, grey stick; C-chain part of Pr-thiolates, H atoms, associated solvents and anions are omitted.

temperatures, the reduction process was deliberately decelerated, facilitating the growth of high-quality crystals. This method distinguishes itself from the previously reported methods.^{19,20}

The red-colored crystals were analyzed using single-crystal X-ray diffraction data (SCXRD), which revealed that they belong to the trigonal crystal system with a space group of $R\bar{3}$ (Table S1, ESI†). The crystal structure is composed of fifty-eight Cu atoms, thirty-six SPr, and eight PPh_3 units. Based on the crystal structural analysis, the synthesized NC is $[\text{Cu}_{58}(\text{SPr})_{36}(\text{PPh}_3)_8]$, as depicted in Fig. 1. Fig. S2 (ESI†) displays the thermal ellipsoid for each atom, and the structure as a whole exhibits a 3-fold rotation axis, as depicted in Fig. S3 (ESI†).

Detailed structural analysis reveals that the cluster exhibits a core-shell configuration. We differentiate the core from the shell depending on their connectivity to the surface-protecting ligands. We identified that eight Cu atoms form a cubic core geometry where the average Cu–Cu distance is 2.654 ± 0.004 Å (Fig. 2a and Table S2, ESI†). The Cu–Cu distance is a little bit longer than that of the metallic Cu, which differs to be considered as a metallic bond.¹³ However, the strong

interaction between the Cu atoms at the core can be attributed to the cuprophilic interaction, as this distance is much lower than twice the van der Waals radius of Cu. Considering the polyhedral architecture, the core geometry falls under the Platonic solid with six faces and eight vertices configured as 4.4.4 and the point group symmetry of this core geometry is octahedral. The core is further connected with the outer shell by Cu–Cu interactions without any involvement of the thiolate linkage (Fig. S4, ESI†). Furthermore, we consider the shell layer based on the geometry of each layer and its distance from the Cu_8 cubic core. This consideration produces four Cu shells by differentiating three middle layers and one outer layer. The radius of each shell in the Cu_{58} NC approximately increases from 3.3 Å to 7.3 Å to encapsulate the geometry of the previous shell. However, some of the Cu–Cu distances in these shells exceed twice the van der Waals radius; so we treat those interactions as virtual and represent them as dotted lines, while the major interactions are represented as solid lines. The first shell of the Cu_{58} NC comprises six Cu atoms arranged in an octahedral geometry through virtual connections where each Cu atom is positioned by capping each facet of the Cu_8 cubic core (Fig. 2b and Fig. S4, ESI†). The average distance between the Cu_8 cubic core and Cu_6 octahedral shell layer is 2.748 ± 0.009 Å. Regarding its polyhedral architecture, the geometry of the first shell falls under a Platonic solid category with eight triangular faces and six vertices arranged in a 3.3.3.3 configuration, displaying an octahedral point group. The second shell in the middle layer of the Cu_{58} NC comprises twenty-four Cu atoms arranged in a rhombicuboctahedron geometry, where both real and virtual bonds exist between the Cu atoms (Fig. 2c). It has been observed that four Cu_6 units are virtually connected diagonally to form this geometric structure. Furthermore, each Cu_6 unit is constructed by capping each corner of the Cu_8 cubic core and maintains an average distance of 2.703 ± 0.017 Å to the first shell and an average distance of 2.771 ± 0.030 Å to the previous shell (Fig. S4, ESI†). The architecture of this Cu_{24} shell resembles an Archimedean solid with 26 faces (eight triangles and eighteen squares) and twenty-four vertices arranged in a 3.4.4.4 configuration and exhibiting an octahedral point group. The third shell and the final layer in the middle of the Cu_{58} NC are composed of twelve Cu atoms arranged in a cuboctahedron geometry through virtual connections (Fig. 2d). The Cu atoms in this shell are placed at the midpoints of the Cu_8 cubic core edges (Fig. S4, ESI†). The architecture of this Cu_{12} shell resembles that of another Archimedean solid, with fourteen faces, (eight triangles and six squares) and twelve vertices arranged in a 3.4.3.4 configuration, exhibiting an octahedral point group. The average separation distance between the previous shell is 2.748 ± 0.024 Å. The fourth shell, which is the outermost, comprises eight Cu atoms arranged in a cubic geometry *via* virtual connections (Fig. 2e). Each Cu atom is located diagonally to the Cu_8 cubic core (Fig. S4, ESI†). Similar to the core, the architecture of this outermost Cu_8 shell also exhibits a Platonic solid-like structure with the same number of faces and vertices. The Cu_{58} NC consists of a platonic core and four shells, each displaying

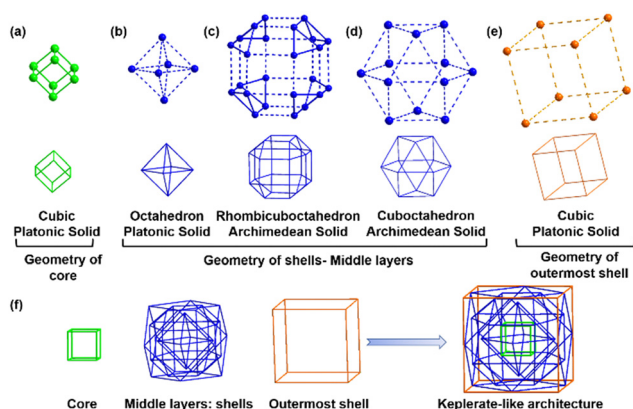


Fig. 2 Nested arrangement of Cu atoms inside the cluster: (a) Cu_8 cubic core, (b) Cu_6 octahedron shell, (c) Cu_{24} rhombicuboctahedron shell, (d) Cu_{12} cuboctahedron shell, (e) outermost Cu_8 cubic shell and (f) formation route of the Keplerian architecture through the arrangement of Cu atoms. Color legend: Cu, light green, blue and brown.



geometries from both platonic and Archimedean solids. Interestingly, all of these geometries possess similar local octahedral symmetry, which allows for easy alignment of the metallic architecture inside the cluster through the global rotational axis, accommodating the core and shells together without any issues. Thus, it can be concluded that the metallic architecture of Cu_{58} NC comprises five concentric nested polyhedra, thanks to the compatible symmetry of each polyhedron. John Conway, a mathematician from the past, developed a model called “Kepler’s Kosmos” which arranges the five Platonic solids in a particular way.¹ However, aligning the Platonic and Archimedean solids on a nanoscale is a more complex task. Nevertheless, in this case, a comparable number of copper layers (Cu_8 core, Cu_6 shell, Cu_{24} shell, Cu_{12} shell, and Cu_8 shell) are concentrically aligned, suggesting that the arrangement of copper atoms is similar to that of Kepler’s Kosmos (Fig. 2f).

The layers were differentiated into middle and outer layers based on their connectivity. The middle layers were found to be connected to each other through Cu–Cu interactions and thiol bridging. On the other hand, the outer layer was only connected to the middle layers through thiol bridging, as shown in Fig. S5 (ESI†). However, we observed that many times, the Cu–Cu distances in the shells were greater than twice the van der Waals radius of Cu, indicating a lack of strong cuprophilic interactions. This raised questions about the mechanism that keeps Cu atoms in their positions. To investigate this issue, we examined the presence of anionic groups in the preferred positions, which appeared to play a role in keeping the Cu atoms in their intact positions. Two anion shells were identified, which were formed by the surface-protecting thiolate ligands. Both of these shells were positioned outward from the metallic part and a virtual bonding between the two anions was established using dotted lines. The small anionic shell contained twelve thiolates (S_{12}) that protected the Cu_8 cubic core at the facets, forming an icosahedral geometry with twenty faces and twelve vertices with an icosahedral point group (Fig. 3a). Each thiolate ligand was connected through μ_4 bridging with $\eta^1, \eta^1, \eta^1, \eta^1$ connectivity to the middle layers (Fig. S5, ESI†). We found that each of these thiolate ligands was connected with the first and third shells with μ_1 and μ_1 bridging mode, respectively, whereas the second shell was linked by μ_2 bridging mode, with the Cu–S bond length ranging

from 2.263(4) to 2.441(5) Å (Table S3, ESI†). The average inner-sphere radius of this anionic shell was 4.0423 ± 0.708 Å. The second and larger anionic shell had an average mid-sphere radius of 6.5675 ± 0.272 Å and contained twenty-four thiolate ligands protecting the Cu_8 cubic core at the edges. The twenty-four thiolate ligands (S_{24}) adopted a truncated cube-like Archimedean solid geometry with fourteen faces (eight triangles and six octagons) and twenty-four vertices with an octahedral point group (Fig. 3b). Each of the thiolate ligands in this shell was connected through μ_3 bridging with η^1, η^1, η^1 connectivity to the Cu shells (Fig. S5, ESI†). We found that these connections existed between Cu shell 2, shell 3, and shell 4, with Cu–S bond lengths ranging from 2.223(4) to 2.385(4) Å. In addition to this anionic shell, eight PPh_3 ligands formed a cubic arrangement of P_8 by capping the terminal Cu atoms, with Cu–P bond lengths ranging from 2.239(4) to 2.239(7) Å (Fig. 3c).

In accordance with the crystallographic structure, there is much more information left about this NC that remains to be revealed. It is well known that Cu(I) is more resistant to reduction than Au(I) or Ag(I). Consequently, when a Cu(I) precursor is reduced with a hydride source – a common method of synthesizing Ag and Au NCs – stable Cu(I) hydride clusters are often formed. However, these hydrides are not detectable by SCXRD. Hydrides in this study were confirmed using ESI-MS measurements, where a peak at m/z 4253.65 aligned well with the simulated pattern (Fig. 4a). The isotropic distribution in the ESI-mass spectrum, with a peak separation of $m/z = 0.5$, confirmed the 2+ charge of the cluster unit. To determine the origin of the hydrides, a Cu_{58}D NC was synthesized using

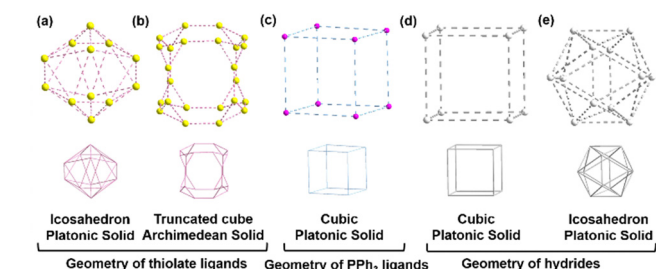


Fig. 3 The arrangement of the ligand shells: (a) S_{12} icosahedron anionic shell, (b) S_{24} truncated cubic shell, (c) P_8 cubic shell, (d) H_8 cubic shell and (e) H_{12} icosahedron shell. Color legend: S, yellow; P, violet; and H, white.

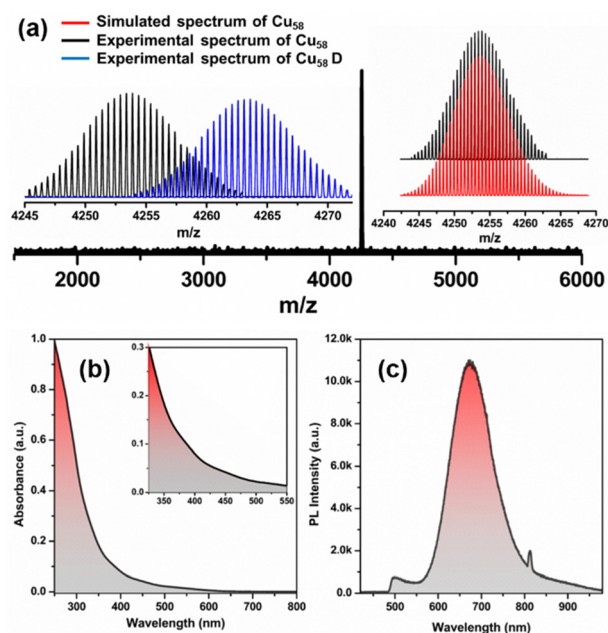


Fig. 4 (a) ESI-mass spectrum in positive mode confirming the presence of hydrides with the matching of the molecular peak and simulated one, with the inset showing the difference in the molecular peak positions between Cu_{58} NC and Cu_{58}D , (b) UV-vis absorbance peak of Cu_{58} NC dissolved in CHCl_3 medium and (c) corresponding emission peak upon excitation at 405 nm.



NaBD₄, which resulted in a shift in the ESI-mass spectrum with an increase of *m/z* value by 9.7, confirming that all hydrides originate from the reducing agent during the synthesis of Cu₅₈ NCs (Fig. 4a inset and Fig. S6, ESI†). Therefore, it is hypothesized that the reduction of a Cu(I) salt in a mixed ligand environment would lead to the formation of stable Cu(I) NCs.

To locate the 20 hydrides, we employed a machine-learning approach and the most probable configuration was confirmed by density functional theory (DFT) geometry optimization (Fig. S7, S8 and Table S4, ESI†). All hydrides are bridged between the core and middle layers, with eight of them connected through a μ_4 bridging mode at the eight vertices of the Cu₈ cubic core in an outward direction, while the remaining twelve are connected through μ_5 bridging mode at each edge of the Cu₈ cubic core in the outward direction (Fig. S9, ESI†). The arrangement of eight hydrides (H₈) forms a cubic geometry, while the arrangement of twelve hydrides (H₁₂) forms an icosahedral geometry (Fig. 3d and e). So, the structure overall comprises five Cu(I) polyhedral geometries and five ligand geometries. Bader charge analysis confirmed the cationic nature of every Cu atom and the anionic nature of hydrogen atoms (Table S5, ESI†). To identify the photo physical properties of this Cu₅₈ NC, we dissolved it in chloroform and used steady-state UV-vis absorbance and photoluminescence spectroscopic measurements. The UV-vis absorbance showed a monotonic decrease without any prominent peaks, indicating an electronic transition from ligand to metal, which is well matched with the previously reported Cu(I) NCs (Fig. 4b).^{20,21} The HOMO at −1.5263 eV was found to be triply degenerate and composed primarily of thiolate and hydride ligands and this is representative of other filled orbitals, while the LUMO at −0.0045 eV was mainly constructed from the Cu₈ cubic core (Fig. S10, ESI†). Interestingly, Cu-thiolate NCs do not show luminescence at room temperature when the number of Cu atoms exceeds 20.^{17,19,22} However, we observed red emission with a maximum intensity of 673 nm when exciting a chloroform solution of Cu₅₈ NC at 405 nm (Fig. 4c) with a relative quantum yield of 0.38. It has an average emission lifetime of 1.42 μ s, as determined by time-correlated single photon counting experiments (Fig. S11 and Table S6, ESI†). Thus, it is evident that highly symmetric nested NCs not only possess fascinating structural architecture but also demonstrate distinct photophysical properties in comparison to their counterparts.

In conclusion, we successfully synthesized a Cu(I) NC with a highly symmetric structure consisting of five concentric nested polyhedral architectures, protected by thiolate and phenyl phosphonate ligands on its surface. Although the hydrides were not detected by SCXRD, their presence was confirmed by ESI-MS and their positions were determined by machine-learning coupled with DFT. The ordered geometric arrangement of each ligand and hydride also resembles the symmetric arrangement of the Cu atoms, making this structure highly organized. The step-by-step structural understanding of our

work may inspire researchers to synthesize other highly symmetric metallic nanoclusters with required photophysical properties.

This work was financially supported by the Japan Society for the Promotion of Science (JSPS) KAKENHI (grant no. 20H02698 and 20H02552), and the Scientific Research on Innovative Areas “Aquatic Functional Materials” (grant no. 22H04562).

Conflicts of interest

There are no conflicts to declare.

Notes and references

- 1 Y.-M. Su, Z. Wang, C.-H. Tung, D. Sun and S. Schein, *J. Am. Chem. Soc.*, 2021, **143**, 13235–13244.
- 2 Y.-M. Su, Z. Wang, S. Schein, C.-H. Tung and D. Sun, *Nat. Commun.*, 2020, **11**, 3316.
- 3 P. Cromwell, Cambridge University Press, Cambridge, 1997, pp. 51–94.
- 4 Y. He, T. Ye, M. Su, C. Zhang, A. E. Ribbe, W. Jiang and C. Mao, *Nature*, 2008, **452**, 198–201.
- 5 Y. Liu, C. Hu, A. Comotti and M. D. Ward, *Science*, 2011, **333**, 436–440.
- 6 X. Ma, Y. Bai, Y. Song, Q. Li, Y. Lv, H. Zhang, H. Yu and M. Zhu, *Angew. Chem., Int. Ed.*, 2020, **59**, 17234–17238.
- 7 S. Biswas, A. K. Das, A. C. Reber, S. Biswas, S. Bhandary, V. B. Kamble, S. N. Khanna and S. Mandal, *Nano Lett.*, 2022, **9**, 3721–3727.
- 8 R. Jin, C. Zeng, M. Zhou and Y. Chen, *Chem. Rev.*, 2016, **116**, 10346–10413.
- 9 W. Krätschmer, L. D. Lamb, K. Fostiropoulos and D. R. Huffman, *Nature*, 1990, **347**, 354–358.
- 10 Z. Wang, H.-F. Su, Y.-Z. Tan, S. Schein, S.-C. Lin, W. Liu, S.-A. Wang, W.-G. Wang, C.-H. Tung and D. Sun, *Proc. Natl. Acad. Sci. U. S. A.*, 2017, **114**, 12132–12137.
- 11 A. Baghadasaryan and T. Bürgi, *Nanoscale*, 2021, **13**, 6283–6340.
- 12 I. Chakraborty and T. Pradeep, *Chem. Rev.*, 2017, **117**, 8208–8271.
- 13 B.-L. Han, Z. Liu, L. Feng, Z. Wang, R. K. Gupta, C. M. Aikens, C.-H. Tung and D. Sun, *J. Am. Chem. Soc.*, 2020, **142**, 5834–5841.
- 14 T.-A. D. Nguyen, Z. R. Jones, D. F. Leto, G. Wu, S. L. Scott and T. W. Hayton, *Chem. Mater.*, 2016, **28**, 8385–8390.
- 15 S. Lee, M. S. Bootharaju, G. Deng, S. Malola, W. Baek, H. Hakkinen, N. Zheng and T. Hyeon, *J. Am. Chem. Soc.*, 2020, **142**, 13974–13981.
- 16 C. Sun, N. Mammen, S. Kaappa, P. Yuan, G. Deng, C. Zhao, J. Yan, S. Malola, K. Honkala, H. Häkkinen, B. K. Teo and N. Zheng, *ACS Nano*, 2019, **13**, 5975–5986.
- 17 A. Ghosh, R.-W. Huang, B. Alamer, E. Abou-Hamad, M. N. Hedhili, O. F. Mohammed and O. M. Bakr, *ACS Mater. Lett.*, 2019, **1**, 297–302.
- 18 S. Nematullov, R.-W. Huang, J. Yin, A. Shkurenko, C. Dong, A. Ghosh, B. Alamer, R. Naphade, M. N. Hedhili, P. Maity, M. Eddaoudi, O. F. Mohammed and O. M. Bakr, *Small*, 2021, **17**, 2006839.
- 19 C. Dong, R.-W. Huang, C. Chen, J. Chen, S. Nematullov, X. Guo, A. Ghosh, B. Alamer, M. N. Hedhili, T. T. Isimjan, Y. Han, O. F. Mohammed and O. M. Bakr, *J. Am. Chem. Soc.*, 2021, **143**, 11026–11035.
- 20 A. K. Das, S. Biswas, V. S. Wani, A. S. Nair, B. Pathak and S. Mandal, *Chem. Sci.*, 2022, **13**, 7616–7625.
- 21 P. Yuan, R. Chen, X. Zhang, F. Chen, J. Yan, C. Sun, D. Ou, J. Peng, S. Lin, Z. Tang, B. K. Teo, L.-S. Zheng and N. Zheng, *Angew. Chem., Int. Ed.*, 2019, **58**, 835–839.
- 22 X. Lin, J. Tang, C. Zhu, L. Wang, Y. Yang, H. Fan, C. Liu and J. Huang, *Chem. Sci.*, 2023, **14**, 994–1002.
- 23 R. Jin, C. Liu, S. Zhao, A. Das, H. Xing, C. Gayathri, Y. Xing, N. L. Rosi, R. R. Gil and R. Jin, *ACS Nano*, 2015, **9**, 8530–8536.

